Observation of high-T_c superconductivity in rectangular FeSe/SrTiO$_3$(110) monolayers

P. Zhang,[1,=] X.-L. Peng,[1,=] T. Qian,[1,2,=] P. Richard,[1,2,=] X. Shi,[1] J.-Z. Ma,[1] B. B. Fu,[1] Y.-L. Guo,[1] Z. Q. Han,[1,3] S. C. Wang,[3]
L. L. Wang,[2,4] Q.-K. Xue,[2,4] J. P. Hu,[1,2,5] Y.-J. Sun,[1,*] and H. Ding[1,2,†]

[1]*Beijing National Laboratory for Condensed Matter Physics and Institute of Physics, Chinese Academy of Sciences, Beijing 100190, China*
[2]*Collaborative Innovation Center of Quantum Matter, Beijing, China*
[3]*Department of Physics, Renmin University, Beijing 100872, China*
[4]*State Key Laboratory of Low-Dimensional Quantum Physics, Department of Physics, Tsinghua University, Beijing 100084, China*
[5]*Department of Physics, Purdue University, West Lafayette, Indiana 47907, USA*

We design a monolayer film of FeSe on SrTiO$_3$(110) substrate [FeSe/STO(110)], with a C$_2$ symmetry induced by epitaxial strain. Compared to FeSe on SrTiO$_3$(001) substrate [FeSe/STO(001)], one of the in-plane lattice constants is reduced by 6%, to ∼3.67 Å. FeSe/STO(110) exhibits a large nearly isotropic superconducting gap of 16 meV filled around 60 K, similar to those obtained on FeSe/STO(001) films. Our results strongly suggest that the lattice C$_4$ symmetry is not essential for reaching high T_c's in Fe-based superconductors and pose a new challenge to theory.

The maximum superconducting (SC) critical temperature T_c in iron-based superconductors appears in the tetragonal structure [1,2]. For instance, the T_c of bulk FeSe jumps from 8 to 37 K upon suppression of an orthorhombic distortion by application of external pressure [3,4]. Similarly, the recently discovered FeSe monolayers grown by molecular beam epitaxy on SrTiO$_3$(001) substrates [FeSe/STO(001)], which have the highest T_c (65 K) among all Fe-based materials, are characterized by a C$_4$ axis [5–9]. In principle, epitaxial strain on superconductivity films can be used to change the lattice and symmetry of high-T_c superconductors. For example, superconductivity in La$_{2-x}$Sr$_x$CuO$_4$ film is suppressed under tensile strain but enhanced under compressive strain [10,11]. The T_c value can be changed by 30% to 100% when the lattice constants show a 3% difference. However, the anisotropic in-plane strain effect is seldom investigated because the strain rapidly decays when the film thickness increases. High-T_c FeSe monolayers provide an opportunity to study the effect of anisotropic strain.

Here we study the symmetry-broken state of FeSe/STO (110) induced by ∼6% epitaxial strain and show that high T_c can also be achieved in a C$_2$ symmetric iron-based superconductor. The characterization of the Fermi surface (FS) using angle-resolved photoemission spectroscopy (ARPES) indicates an even higher anisotropy for the band structure. Nevertheless, we observed a nearly isotropic SC gap of about 16 meV that closes around 60 K, which is very similar to what is observed for the square films. This result proves that although a distortion breaking the symmetry of the Fe-Fe directions (B$_{1g}$) might be detrimental to superconductivity, the SC properties are not necessarily affected by a distortion that keeps the Fe-Fe directions equivalent (B$_{2g}$).

Atomically flat, 0.7 wt% Nb-doped STO(110) substrates were obtained after annealing for 6 h at 600 °C and then 1.5 h

at 950 °C. In order to grow FeSe films, Fe (99.98%) and Se (99.999%) were coevaporated from Knudsen cells at a flux ratio of 1:10, which were measured with a quartz crystal balance, with a growth rate of 0.35 UC/min. Substrates were kept at 310 °C during FeSe film growth. After growth, FeSe monolayer films were annealed at 365 °C for 8 h to improve the crystallinity and subsequently transferred *in situ* to the ARPES chamber of our molecular beam epitaxy–ARPES combined system at the Institute of Physics, Chinese Academy of Sciences. Reflection high-energy electron diffraction (RHEED) pictures of the FeSe monolayer films [Fig. 1(a)] and scanning-tunneling-microscopy topographic images [Fig. 1(b)] suggest high-quality films. ARPES measurements were performed in the same combined system using an R4000 analyzer with a helium discharge lamp and at the "Dreamline" beamline of the Shanghai Synchrotron Radiation Facility using a VG-Scienta D80 electron analyzer. The energy resolution was set to ∼5 meV for gap measurements and ∼15 meV for band structure and FS mapping. The base pressure was 3×10^{-10} Torr in the molecular beam epitaxy chamber and better than 3×10^{-11} Torr during ARPES measurements. Monolayer films of FeSe/STO(110) have also been grown at Tsinghua University using the same method [12]. The high-resolution scanning-tunneling-microscopy spectra obtained for these samples are consistent with the ARPES data presented here.

In contrast to STO(001) substrate, which exposes a tetragonal surface of lattice parameter $a = 3.905$ Å for growth, STO(110) exposes a surface with characteristic lengths a and $\sqrt{2}a$. The huge lattice mismatch between the STO(110) surface and FeSe (3.765 Å [14]) does not allow one-unit-cell to one-unit-cell growth as in the case of FeSe/STO(001). The LEED pattern of our samples [Fig. 1(c)] indicates clearly an orthorhombic structure with an anisotropy of ∼5%, which is consistent with three unit cells of FeSe growing on the top of two STO(110) unit cells, as illustrated in Fig. 1(d). Consequently, this means that the FeSe monolayer is characterized by lattice parameters a and $\frac{2}{3}\sqrt{2}a = 0.94a$. Compared to tetragonal FeSe/STO(001), this orthorhombic distortion in FeSe/STO(110) leads to a 6% compression along

*yjsun@iphy.ac.cn
†dingh@iphy.ac.cn
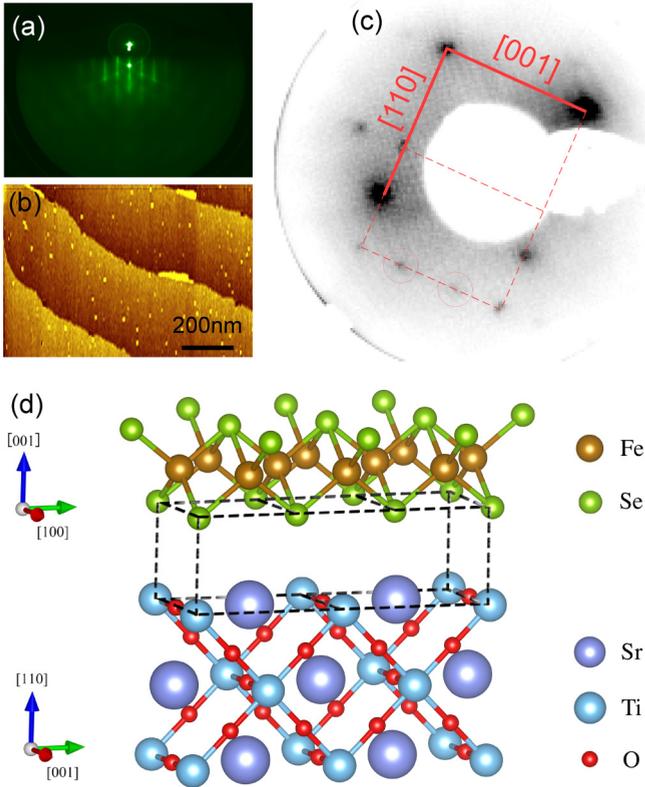=These authors contributed equally to this work.

FIG. 1. (a) RHEED pattern image of a FeSe/STO(110) film. (b) Scanning-tunneling-microscopy tomography image of an FeSe/STO(110) film. (c) LEED pattern of FeSe/STO(110) at 170 K. The Brillouin zone (BZ) of the FeSe film is indicated by solid lines, while dashed lines indicate the BZ of the STO substrate projected on the (110) surface. Red circles correspond to well-known 3×1 surface reconstruction on STO(110) surface [13]. (d) Crystal structure of an FeSe monolayer on top of a STO(110) substrate. Dashed lines indicate the possible match between the FeSe film and the STO(110) substrate.

one axis, corresponding to the in-plane projection of the Fe-Se bonding ([110] direction of the substrate), in agreement with our analysis of the LEED pattern.

The large lattice distortion induced by the STO(110) substrate should have a significant impact on the electronic structure of the FeSe films. The compression of the unit cell enlarges the Brillouin zone along M-Y and consequently elongates the M-centered electron pockets along that same direction. To check whether this is really the case, we performed ARPES measurements on both FeSe/STO(110) and FeSe/STO(001). The comparison of the electronic band structures is shown in Fig. 2. As previously reported [6–9], the FS of FeSe/STO(001) consists of one doubly degenerate circular electron pocket centered at M. Consequently, the samples are highly electron doped compared to bulk FeSe single crystals, for which both hole and electron pockets are measured previously [15–18]. In contrast to FeSe/STO(001), the FS of FeSe/STO(110) is not circular but rather elliptical, with the long axis of the ellipse parallel to M-Y, rather than along Γ-M as in the other Fe-based superconductors.

The FSs of our FeSe/STO(110) and FeSe/STO(001) samples differ not only in shape, but also in size, the latter's being

larger. According to the Luttinger theorem, this indicates a lower electron doping level in FeSe/STO(110). Assuming that each FS is degenerate, we estimate that the doping level of FeSe/STO(110) is 8.6%/Fe, whereas it is about 11.0% for FeSe/STO(001). This difference in doping levels is also evident from the band dispersions. Indeed, the hole band at Γ and the electron band at M are shifted towards lower binding energies (~30 meV at Γ and ~15 meV at M) in FeSe/STO(110) compared to FeSe/STO(001). One possible explanation for the difference in doping is the smaller number of oxygen atoms exposed on the STO(110) surface compared to the STO(001) surface, which may affect the electron transfer caused by oxygen vacancies on the surface of the substrate.

In Figs. 3(a1)–3(a3), we show the temperature evolution of the band structure at the M point of monolayer FeSe/STO(110). Changes mainly occur near the Fermi level (E_F). At 17 K, we see a gap feature that becomes more obvious after dividing the spectrum by the Fermi-Dirac function [Fig. 3(b1)]. No such gap is observed at 70 K [Fig. 3(b3)]. To extract the gap size, we followed the common practice consisting of symmetrizing the energy distribution curves (EDCs) at the Fermi wave vector (k_F), which removes the Fermi-Dirac cutoff, as shown in Fig. 3(c). We normalized all the symmetrized EDCs from −0.1 to 0.1 eV to satisfy spectral weight conservation. We further subtracted the data at 70 K, used as a background [Fig. 3(d)]. Since the coherent peak becomes weaker and broader with increasing temperature, we used a phenomenological model to extract the gap size Δ [19], in which we consider the self-energy $\Sigma(\mathbf{k},\omega) = -i\Gamma_1 + \Delta^2/[(\omega + i0^+) + \varepsilon(\mathbf{k})]$, where ω is the energy, $\varepsilon(\mathbf{k})$ is the electronic band dispersion, and Γ_1 is a constant single-particle scattering rate. The spectral function $A(\mathbf{k},\omega)$ is defined by $\pi A(\mathbf{k},\omega) = \Sigma''(\mathbf{k},\omega)/[(\omega - \varepsilon(\mathbf{k}) - \Sigma'(\mathbf{k},\omega))^2 + \Sigma''(\mathbf{k},\omega)^2]$, where Σ' and Σ'' are the real and imaginary parts of the self-energy, respectively, and $\varepsilon(\mathbf{k}_F) = 0$. After convoluting the spectral function by the instrumental resolution function, we can fit the data at $\mathbf{k} = \mathbf{k}_F$ and extract Δ, which is contained in Σ'. The results are displayed in Figs. 3(e) and 3(h) for FeSe/STO(110) and FeSe/STO(001), respectively. A nearly-temperature-independent gap size of about 16 meV is found in FeSe/STO(110) below T_c [Fig. 3(e)]. For FeSe/STO(001) we see a small temperature dependence of the gap, which is about 10 meV at the lowest temperature.

Because the gap looks more filling than closing with temperature, we also used data from Fig. 3(d) to extract the spectral weight loss, defined as the area between the high-temperature background (70 K) and the symmetrized EDCs, which is also equal, below T_c, to the weight of the coherent peak. A similar procedure was successfully used in the past [20] to investigate the SC gap and the pseudogap in $(Bi,P)_2(Sr,La)_2CuO_{6+\delta}$. The method is illustrated in the inset in Fig. 3(e). For both FeSe/STO(110) and FeSe/STO(001), the spectral weight loss decreases with increasing temperature, and it vanishes around 60 and 50 K, respectively, which are consistent with the temperatures at which the gap size closes in our fits. We can thus use these values as reliable definitions of T_c. Keeping in mind that the gap size changes with the annealing conditions in FeSe/STO(001) [7], our results on FeSe/STO(110) are very similar, both qualitatively and quantitatively, to results obtained on FeSe/STO(001), also shown in Fig. 3. The gaps in both materials thus have
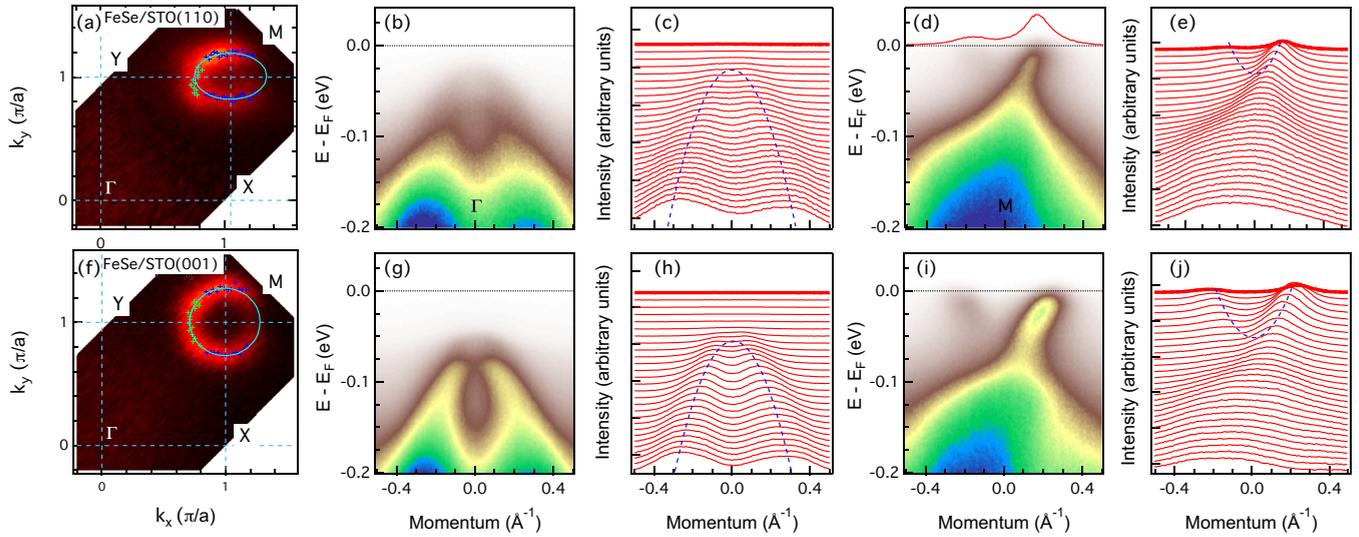
FIG. 2. Top and bottom rows correspond to results obtained on monolayer films of FeSe/STO(110) and FeSe/STO(001), respectively. Data are recorded at 35 K with a He discharge lamp. (a, f) FS. Blue and green dots are maxima of the intensity map along the vertical and horizontal directions, respectively. Light-blue curves are elliptical fittings of these dots. (b, g) ARPES intensity cut along a cut passing through the Γ point. (c, h) Momentum distribution curves (MDCs) of (b) and (g), respectively. The dotted blue line is a guide for the eye for the main band dispersion. (d, i) Same as (b) and (g), but for a cut passing through M. The red curve in (d) is the MDC at E_F. (e, j) MDCs of (d) and (i), respectively.

the same origin, and hereafter, following previous reports on FeSe/STO(001) [6–9], we refer to them as SC gaps.

To check how the gap size evolves along the anisotropic FS of FeSe/STO(110), we measured the gap amplitude at different momentum locations along the FS, as shown in the inset in Fig. 3(i). Surprisingly, we observe a rather isotropic gap, as illustrated by the polar distribution of the gap in Fig. 3(i). In other words, not only does superconductivity with a large SC

gap survive to the C_2 lattice distortion, but there is no obvious imprint of the lattice distortion on the gap distribution. As a corollary, the C_4 symmetry is not essential for reaching high T_c values in Fe-based superconductors. We also note that it has been proposed that when different SC order parameters have comparable free energies, the breakdown of the C_4 symmetry may increase T_c by mixing these SC order parameters, thus lifting the pairing frustration [21].
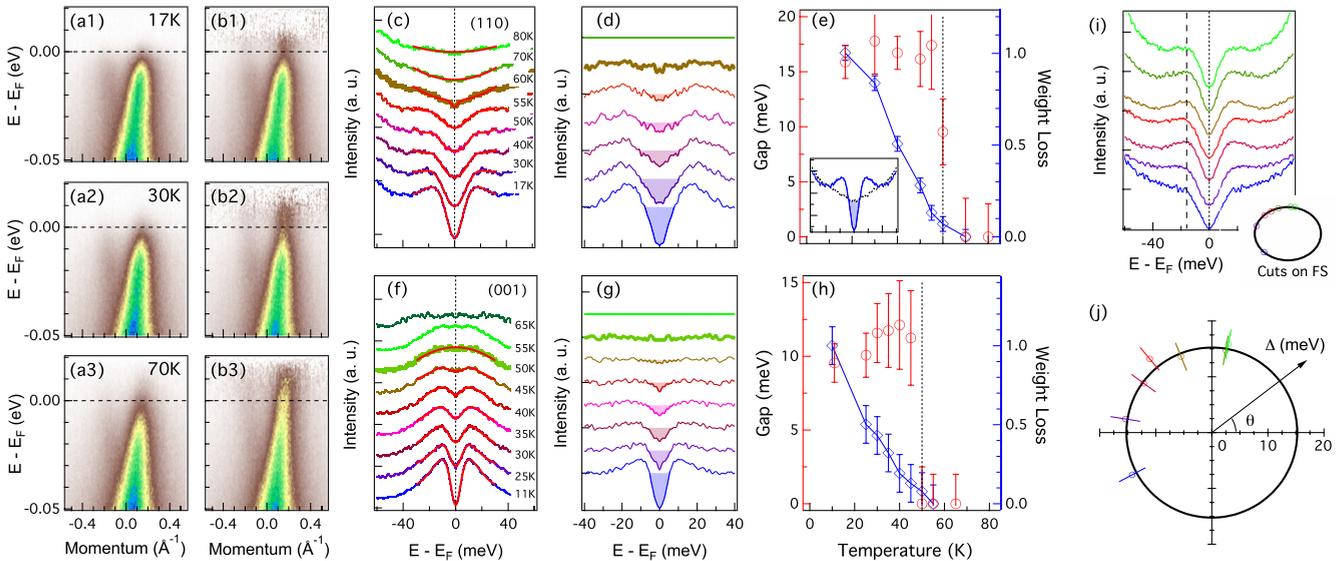

FIG. 3. (a1–a3) Band structure of FeSe/STO(110) at M recorded at different temperatures. (b1–b3) Same as (a1)–(a3), but divided by the Fermi-Dirac function. (c, f) Temperature evolution of the symmetrized energy distribution curves (EDCs) at k_F of FeSe/STO(110) and FeSe/STO(001), respectively. Tick red curves are fitting results using a model described in the text. (d, g) Corresponding symmetrized EDCs after subtraction of the high-temperature background. Shaded areas correspond to the difference between the background and the data, as illustrated in the inset in (e). (e, h) Gap size and spectral weight loss as a function of temperature in FeSe/STO(110) and FeSe/STO(001), respectively. The gap is obtained from the fits shown in (c) and (f). (i) Momentum distribution of the EDCs recorded at 17 K on the FS of FeSe/STO(110); (j) the corresponding polar representation of the SC gap amplitude. The inset in (i) shows the momentum locations of the EDCs.
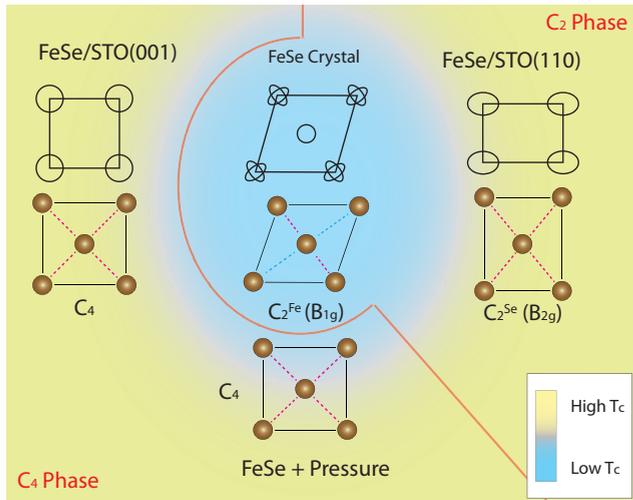
FIG. 4. Superconductivity in the different forms of FeSe (only Fe atoms shown), with their corresponding FSs. The relative T_c is given by the background color. Dashed color lines indicate which Fe-Fe bondings are equivalent.

FeSe monolayer films share many similarities with bulk $K_x Fe_{2-y} Se_2$ [22], (Li,Fe)OHFeSe [23], gate-voltage tuned bulk FeSe [24], and potassium-doped bulk FeSe [25]. Therefore, the origin of superconductivity in the films is likely similar to that in these bulk materials. The different crystal structures of SC FeSe, with the corresponding schematic FSs, are summarized in Fig. 4. The C_2 distortion observed in FeSe/STO(110), which we hereafter refer to as C_2^{Se} distortion (B_{2g} irreducible representation for the square lattice with Fe atoms only), is different from the C_2^{Fe} distortion (B_{1g}) observed in bulk FeSe [4] and in the parent compounds of many ferropnictide families [26,27]. In the latter case, the distortion induces inequivalent Fe-Fe bondings in perpendicular directions, which stabilizes the long-range stripe spin-density-wave order in $BaFe_2As_2$ [28] and the long-range orbital ordering in bulk FeSe [4]. Since these long-range orderings are associated with order parameters competing with superconductivity [29], the C_2^{Fe} distortion is likely an obstacle for achieving high-T_c superconductivity. While the C_2^{Se} distortion is related to a bicollinear spin-density-wave order in bulk FeTe [30], such an electronic order is not observed in FeSe/STO(110). Therefore, our results show that high-T_c superconductivity is unaffected by the B_{2g} distortion. The SC pairing mechanism is probably tied to the electronic degrees of freedom, like spin [31,32]

and orbital [33]. One of the commonly used models, the so-called J_1-J_2-J_3 model, has been proved very useful in explaining the SC gap symmetry in Fe-based superconductors [34,35]. We point out that the C_2^{Se} distortion described here induces inequivalent next-neighboring distances, and thus the spin exchange term J_2 splits into the inequivalent terms J_{2a} and J_{2b}, though we have no way to determine *ab initio* the ratio J_{2a}/J_{2b}. The rather isotropic gap observed in this system suggests that either the anisotropy of J_2 is low or its influence on gap anisotropy is negligible.

In a previous ARPES report [9], the observation of a band replica has been attributed to a strong coupling with a surface phonon of STO(001), which could play an important role in boosting the T_c of FeSe/STO(110). Although we did not observe such a replica in our FeSe/STO(110) samples, we can neither exclude nor prove that a similar mechanism occurs, but explaining why FeSe/STO(110) and FeSe/STO(001) have similar T_c's and gap sizes would require the "boosting phonons" to involve the same vibrations of atoms along the surface of the substrate. Nevertheless, strong empirical conclusions emerge from our comparative work on FeSe/STO(110) and FeSe/STO(001) monolayer films: (1) A large electron doping is necessary for achieving a high T_c in ferrochalcogenide materials, possibly by pushing the Γ-centered hole pockets below E_F. Indeed, superconductivity has been achieved in three-monolayer-thick samples of FeSe only after electron doping of their surface with K [36]. (2) C_4 symmetry is not necessary for achieving high T_c and superconductivity is not harmed by a C_2^{Se} distortion that breaks the rotational symmetry but leaves all Fe-Fe bondings equivalent. (3) In principle, the C_2^{Se} distortion induces different J_{2a} and J_{2b}, while the SC gap is still rather isotropic. Therefore, our ARPES observation of high-T_c superconductivity with an isotropic gap in this new type of interfacial material challenges some of the current beliefs and sheds light on the mechanism of Fe-based superconductors.

[1] J. Zhao, Q. Huang, C. de la Cruz, S. Li, J. W. Lynn, Y. Chen, M. A. Green, G. F. Chen, G. Li, Z. Li, J. L. Luo, N. L. Wang, and P. Dai, Nat. Mater. **7**, 953 (2008).

[2] S. Nandi, M. G. Kim, A. Kreyssig, R. M. Fernandes, D. K. Pratt, A. Thaler, N. Ni, S. L. Bud'ko, P. C. Canfield, J. Schmalian, R. J. McQueeney, and A. I. Goldman, Phys. Rev. Lett. **104**, 057006 (2010).

[3] S. Margadonna, Y. Takabayashi, Y. Ohishi, Y. Mizuguchi, Y. Takano, T. Kagayama, T. Nakagawa, M. Takata, and K. Prassides, Phys. Rev. B **80**, 064506 (2009).

[4] K. Miyoshi, K. Morishita, E. Mutou, M. Kondo, O. Seida, K. Fujiwara, J. Takeuchi, and S. Nishigori, J. Phys. Soc. Jpn. **83**, 013702 (2014).

[5] Q.-Y. Wang, Z. Li, W.-H. Zhang, Z.-C. Zhang, J.-S. Zhang, W. Li, H. Ding, Y.-B. Ou, P. Deng, K. Chang, J. Wen, C.-L. Song, K. He, J.-F. Jia, S.-H. Ji, Y.-Y. Wang, L.-L. Wang, X. Chen, X.-C. Ma, and Q.-K. Xue, Chin. Phys. Lett. **29**, 037402 (2012).

[6] D. Liu, W. Zhang, D. Mou, J. He, Y.-B. Ou, Q.-Y. Wang, Z. Li, L. Wang, L. Zhao, S. He, Y. Peng, X. Liu, C. Chen, L. Yu, G.

Liu, X. Dong, J. Zhang, C. Chen, Z. Xu, J. Hu, X. Chen, X. Ma, Q. Xue, and X. J. Zhou, Nat. Commun. **3**, 931 (2012).

[7] S. He, J. He, W. Zhang, L. Zhao, D. Liu, X. Liu, D. Mou, Y.-B. Ou, Q.-Y. Wang, Z. Li, L. Wang, Y. Peng, Y. Liu, C. Chen, L. Yu, G. Liu, X. Dong, J. Zhang, C. Chen, Z. Xu, X. Chen, X. Ma, Q. Xue, and X. J. Zhou, Nat. Mater. **12**, 605 (2013).

[8] S. Tan, Y. Zhang, M. Xia, Z. Ye, F. Chen, X. Xie, R. Peng, D. Xu, Q. Fan, H. Xu, J. Jiang, T. Zhang, X. Lai, T. Xiang, J. Hu, B. Xie, and D. Feng, Nat. Mater. **12**, 634 (2013).

[9] J. J. Lee, F. T. Schmitt, R. G. Moore, S. Johnston, Y. T. Cui, W. Li, M. Yi, Z. K. Liu, M. Hashimoto, Y. Zhang, D. H. Lu, T. P. Devereaux, D. H. Lee, and Z. X. Shen, Nature **515**, 245 (2014).

[10] I. Bozovic, G. Logvenov, I. Belca, B. Narimbetov, and I. Sveklo, Phys. Rev. Lett. **89**, 107001 (2002).

[11] H. Sato, A. Tsukada, M. Naito, and A. Matsuda, Phys. Rev. B **61**, 12447 (2000).

[12] G. Zhou, D. Zhang, C. Liu, C. Tang, X. Wang, Z. Li, C. Song, S. Ji, K. He, L. Wang, X. Ma, and Q.-K. Xue, Appl. Phys. Lett. **108**, 202603 (2016).

[13] B. C. Russell and M. R. Castell, Phys. Rev. B **77**, 245414 (2008).

[14] F.-C. H. Hsu, J.-Y. Luo, K.-W. Yeh, T.-K. Chen, T.-W. Huang, P. M. Wu, Y.-C. L. Lee, Y.-L. Huang, Y.-Y. Chu, D.-C. Yan, and M.-K. Wu, Proc. Natl. Acad. Sci. USA **105**, 14262 (2008).

[15] J. Maletz, V. B. Zabolotnyy, D. V. Evtushinsky, S. Thirupathaiah, A. U. B. Wolter, L. Harnagea, A. N. Yaresko, A. N. Vasiliev, D. A. Chareev, A. E. Böhmer, F. Hardy, T. Wolf, C. Meingast, E. D. L. Rienks, B. Büchner, and S. V. Borisenko, Phys. Rev. B **89**, 220506(R) (2014).

[16] T. Shimojima, Y. Suzuki, T. Sonobe, A. Nakamura, M. Sakano, K. Omachi, J.and Yoshioka, M. Kuwata-Gonokami, K. Ono, H. Kumigashira, A. E. Böhmer, F. Hardy, T. Wolf, C. Meingast, H. v. Löhneysen, H. Ikeda, and K. Ishizaka, Phys. Rev. B **90**, 121111(R) (2014).

[17] M. D. Watson, T. K. Kim, A. A. Haghighirad, N. R. Davies, A. McCollam, A. Narayanan, S. F. Blake, Y. L. Chen, S. Ghannadzadeh, A. J. Schofield, M. Hoesch, C. Meingast, T. Wolf, and A. I. Coldea, Phys. Rev. B **91**, 155106 (2015).

[18] P. Zhang, T. Qian, P. Richard, X. P. Wang, H. Miao, B. Q. Lv, B. B. F. Fu, T. Wolf, C. Meingast, X. X. Wu, Z. Q. Wang, J. P. Hu, and H. Ding, Phys. Rev. B **91**, 214503 (2015).

[19] M. R. Norman, M. Randeria, H. Ding, and J. C. Campuzano, Phys. Rev. B **57**, R11093 (1998).

[20] T. Kondo, R. Khasanov, T. Takeuchi, J. Schmalian, and A. Kaminski, Nature **457**, 296 (2009).

[21] R. M. Fernandes and A. J. Millis, Phys. Rev. Lett. **111**, 127001 (2013).

[22] T. Qian, X.-P. Wang, W.-C. Jin, P. Zhang, P. Richard, G. Xu, X. Dai, Z. Fang, J.-G. Guo, X.-L. Chen, and H. Ding, Phys. Rev. Lett. **106**, 187001 (2011).

[23] L. Zhao, A. Liang, D. Yuan, Y. Hu, D. Liu, J. Huang, S. He, B. Shen, Y. Xu, X. Liu, L. Yu, G. Liu, H. Zhou, Y. Huang, X. Dong, F. Zhou, K. Liu, Z. Lu, Z. Zhao, C. Chen, Z. Xu, and X. J. Zhou, Nat. Commun. **7**, 10608 (2016).

[24] B. Lei, J. H. Cui, Z. J. Xiang, C. Shang, N. Z. Wang, G. J. Ye, X. G. Luo, T. Wu, Z. Sun, and X. H. Chen, Phys. Rev. Lett. **116**, 077002 (2016).

[25] C. H. P. Wen, H. C. Xu, C. Chen, Z. C. Huang, X. Lou, Y. J. Pu, Q. Song, B. P. Xie, M. Abdel-Hafiez, D. A. Chareev, A. N. Vasiliev, R. Peng, and D. L. Feng, Nat. Commun. **7**, 10840 (2016).

[26] M. Rotter, M. Pangerl, M. Tegel, and D. J. Johrendt, Angew. Chem. Int. Ed. **47**, 7949 (2008).

[27] C. de la Cruz, Q. Huang, J. W. Lynn, J. Li, W. Ratcliff, II, J. L. Zarestky, H. A. Mook, G. F. Chen, J. L. Luo, N. L. Wang, and P. Dai, Nature **453**, 899 (2008).

[28] Q. Huang, Y. Qiu, W. Bao, M. A. Green, J. W. Lynn, Y. C. Gasparovic, T. Wu, G. Wu, and X. H. Chen, Phys. Rev. Lett. **101**, 257003 (2008).

[29] R. M. Fernandes, A. V. Chubukov, and J. Schmalian, Nature Phys. **10**, 97 (2014).

[30] Y. Xia, D. Qian, L. Wray, D. Hsieh, G. F. Chen, J. L. Luo, N. L. Wang,, and M. Z. Hasan, Phys. Rev. Lett. **103**, 037002 (2009).

[31] I. I. Mazin, D. J. Singh, M. D. Johannes, and M. H. Du, Phys. Rev. Lett. **101**, 057003 (2008).

[32] K. Seo, B. A. Bernevig, and J. Hu, Phys. Rev. Lett. **101**, 206404 (2008).

[33] H. Kontani and S. Onari, Phys. Rev. Lett. **104**, 157001 (2010).

[34] J. Hu and H. Ding, Sci. Rep. **2**, 381 (2012).

[35] P. Richard, T. Qian, and H. Ding, J. Phys.: Condens. Matter **27**, 293203 (2015).

[36] Y. Miyata, K. Nakayama, K. Sugawara, T. Sato, and T. Takahashi, Nat. Mater. **14**, 775 (2015).